Developing semiclassical Wentzel-Kramers-Brillouin theory for α-$\mathcal{T}_3$ model

Kathy Blaise,[1] Chinedu Ejiogu,[1] Andrii Iurov [1,*] Liubov Zhemchuzhna [1,2] Godfrey Gumbs,[2,3] and Danhong Huang [4,5]

[1]*Department of Physics and Computer Science, Medgar Evers College of City University of New York,*
Brooklyn, New York 11225, USA

[2]*Department of Physics and Astronomy, Hunter College of the City University of New York,*
695 Park Avenue, New York, New York 10065, USA

[3]*Donostia International Physics Center (DIPC), P de Manuel Lardizabal, 4,*
20018 San Sebastian, Basque Country, Spain

[4]*Space Vehicles Directorate, United States Air Force Research Laboratory,*
Kirtland Air Force Base, New Mexico 87117, USA

[5]*Center for High Technology Materials, University of New Mexico, 1313 Goddard SE, Albuquerque, New Mexico 87106, USA*

We developed a complete semiclassical Wentzel-Kramers-Brillouin (WKB) theory for α-$\mathcal{T}_3$ model which describes a wide class of existing pseudospin-1 Dirac cone materials. By expanding the sought wave functions in a series of powers of Planck's constant h, we obtained the leading-order expansion term which is the key quantity required for calculating the electronic and tunneling properties of a semiclassical electron in α-$\mathcal{T}_3$ materials. Based on this, we further derived the WKB transport equations relating two consecutive orders of the wave-function expansion and solved them analytically to obtain the first-order WKB wave function. Meanwhile, we discussed the applicability of the employed approximation as well as how these results could be applied to study various tunneling and transport properties of α-$\mathcal{T}_3$ materials with nontrivial potential profiles. Finally, our results could also be useful for designing next-generation electronic transistors and devices with help from innovative flat-band Dirac materials.

I. INTRODUCTION

The quantum mechanical description of relativistic electronic behavior in various existing materials is predictably a lot more complicated than any classical analysis of such phenomena. Therefore, it is important to build up a semiclassical approximation for high-energy and fast-moving electrons with a simplified formulation, however, could still effectively present a physically correct picture. For this reason, creating a semiclassical Wentzel-Kramers-Brillouin (WKB) theory becomes one of the most important ingredients in studying new types of Hamiltonians, and we firmly believe that by doing so for newly discovered α-$\mathcal{T}_3$ and dice lattices would be deemed as another major advancement in addition to current focused investigations in the field of low-dimensional condensed matter physics [1–7].

Generally speaking, the idea about a WKB approximation aims at finding an approximated solution for a complex differential equation with spatially dependent coefficients, where one of them (e.g., external potential) varies considerably slower than the other ones so that the potential change per de Broglie wavelength of an electron becomes much smaller than its kinetic energy. Consequently, the obtained solution will behave like a rapidly oscillating quantum state modulated by a smooth and nonessential change in an external potential. Practically, the WKB solution can be acquired by expanding the target wave function over the powers of Planck's constant $\hbar$, and therefore, is viewed as a semiclassical approach. This technique was used previously for all Dirac materials, especially for pristine and gapped graphene. WKB theory has numerous applications, including computations of electron tunneling for nontrivial potential barriers [8,9], resonant tunneling and resonant scattering, as well as trapped and localized electronic states [10–12]. The Gutzwiller trace formula has become an important tool in building the semiclassical approximation aiming directly at the density of states [1,13–15]. This approach was applied to the relativistic Dirac Hamiltonian relevant to that in graphene [16] and, specifically, in studying the Berry phases in such materials [17,18]. The WKB approximation in atomic physics with discreet electronic states is explained in Ref. [19] and the Maslov index for Bohr-Sommerfeld quantization was investigated in Refs. [20–22].

As an important case for quantization of electronic states and their semiclassical description, we choose WKB theory under a spatially uniform magnetic field [23]. For zigzag and armchair graphene nanoribbons, the low-energy band structure could be described by an effective Schrödinger Hamiltonian with a double-well potential. Additionally, the WKB solution in graphene with a Coulomb impurity under a strong magnetic field could be expanded by a power series over the effective fine-structure constant [3]. It was previously demonstrated that the method of Gaussian beam summation is

*aiurov@mec.cuny.edu, theorist.physics@gmail.com

045128-1

efficient for building a WKB approximation in the magnetic field for any scalar potential [6]. Semiclassical methods were also applied to address the effect of an electromagnetic wave on magnetoplasmons, an example of which is given by the authors of Ref. [24]. Generally, a WKB method can always be utilized to describe any semiclassical particles with a large kinetic energy. A good description for the application of WKB method was reported even in an very early work, given by Ref. [25].

Specifically, the present work is focused on developing a complete semiclassical WKB theory for the so-called α-$\mathcal{T}_3$ model [26–30]. This model is a general one related to a large group of recently discovered and innovative low-dimensional materials known by the presence of a flat band in their energy dispersions besides a regular Dirac cone. This flat band is stable and sustained under a number of external perturbations, including magnetic and electric fields point defects and even off-resonant dressing fields [31–41].

The atomic structure of α-$\mathcal{T}_3$ materials is represented by a regular hexagon lattice, similar to graphene, with an additional atom at the center of each hexagon. This unique structure leads to the appearance of an extra electron hopping coefficient towards the hub atom from the rim which results in a dispersionless (flat) band in the low-energy band structure of these materials. The significance of this electron hopping from and to the hub atom in a tight-binding model can be quantified by a geometrical phase ϕ ranging continuously from "0" (for graphene) to "$\pi/4$" (for a dice lattice), which is physically associated with single-electron transitions from or to a flat band. Such highly unusual energy dispersions result in novel and truly fascinating electronic [42–49], transport [50–53], optical [54–57], and magnetic [58–64] properties of these innovative materials. Their characteristics are quite different from those in graphene [65]. Together with tilted Dirac cone materials [66–68] and topological Dirac semimetals [69,70], α-$\mathcal{T}_3$ materials are considered to be the most promising and impactful low-dimensional materials at the present time.

So far, a large number of α-$\mathcal{T}_3$ materials and dice lattices were fabricated successfully in laboratory conditions. They included a trilayer $SrTiO_3/SrIrO_3/SrTiO_3$ [71,72], $Hg_{1-x}Cd_x$ quantum well [43,73], Josephson-junction arrays [54,74], Leib and Kagome optical lattices and optical waveguides [75–83], $In_{0.53}Ga_{0.47}As/InP$ semiconducting layers [84], and many other existing materials. A comprehensive review of all these Dirac materials with a flat band can be found in Ref. [85]. For a complete and timely review of all existing flat-band structures, we refer the readers to a recent study [85] reported in 2019, in which the pseudospin-1 Dirac-Weyl Hamiltonian was employed for investigating the electronic behavior in α-$\mathcal{T}_3$ lattices. Meanwhile, the same paper also revealed that the properties of all these materials would display some similarities [86,87]. In fact, both theoretical and experimental investigations on electronic behaviors appear as a hot subject in condensed-matter physics, and nearly all issues related to electrical and optical properties of α-$\mathcal{T}_3$ have already been addressed. Therefore, from a practical perspective, we feel strongly that the building-up of a transparent semiclassical WKB theory for such a new type of material will be beneficial for related experimental and theoretical researches.

The rest of this paper is organized as follows. In Sec. II, we review a low-energy Hamiltonian, its band structure, and electronic states for various types of α-$\mathcal{T}_3$ lattices, including graphene and a dice lattice. Section III, which is a key technical part of the current work, deals with calculating the semiclassical action and longitudinal electron momentum of a WKB model. Consequently, we found wave functions of electrons in successive orders of an $\hbar$-expansion, derived the most general form of transport equations with these expanded electron wave functions, and computed explicitly the first-order wave function so as to verify the applicability of the employed WKB approximation from our Hamiltonian. In Sec. IV, we present a brief discussion on the utilization of our computed semiclassical wave functions for studying electron tunnelings and estimating transmission coefficients as well, by using various nontrivial potential profiles. Finally, we provide some concluding remarks and a outlook in Sec. V.

II. ELECTRONIC STATES IN PSEUDOSPIN-1 DIRAC CONE MATERIALS

In this section, we will establish and apply a semiclassical WKB approximation for an α-$\mathcal{T}_3$ model based on the low-energy electronic states determined from a pseudospin-1 low-energy Dirac-Weyl Hamiltonian

$$\hat{\mathcal{H}}(\boldsymbol{k}|\tau,\phi) = \hbar v_F \begin{bmatrix} 0 & k_-^\tau \cos\phi & 0 \\ k_+^\tau \cos\phi & 0 & k_-^\tau \sin\phi \\ 0 & k_+^\tau \sin\phi & 0 \end{bmatrix}, \quad (1)$$

where $v_F \approx c/100$ represents the Fermi velocity and the geometrical phase ϕ can be obtained from the hopping parameter α through the relation $\alpha = \tan\phi$, while the complex wave numbers $k_\pm^\tau = \tau k_x \pm i k_y$ depend on the valley index $\tau = \pm 1$ representing, respectively, the K and K' valleys. When $\phi = 0$, the Hamiltonian in Eq. (1) reduces to that of graphene. On the other hand, the opposite limit $\phi = \pi/4$ defines a dice lattice, which exhibits the strongest effect from a hub atom and is always treated separately for its importance. Consequently, we will present explicitly results in this paper for the dice lattice.

If free electrons described by Eq. (1) are further subjected to a finite nonuniform potential $V(x)$, such as a square barrier $V(x) = V_0\Theta(x)\Theta(W_B - x)$ or an energy barrier with a non-piecewise-uniform potential profile, the longitudinal momentum $p_x(x)$ will also depend on position x, and the Hamiltonian in Eq. (1) changes to

$$\hat{\mathcal{H}}(\boldsymbol{k}|\tau,\phi) = v_F \hat{\boldsymbol{\Sigma}}^{(3)}(\phi) \cdot \{-i\hbar\boldsymbol{\nabla}_\tau\} + V(x)\hat{\Sigma}_0^{(3)}, \quad (2)$$

where ϕ-dependent 3×3 Pauli matrices $\hat{\boldsymbol{\Sigma}}^{(3)}(\phi) = \{\hat{\Sigma}_x^{(3)}(\phi), \hat{\Sigma}_y^{(3)}(\phi)\}$, and

$$\hat{\Sigma}_x^{(3)}(\phi) = \begin{bmatrix} 0 & \cos\phi & 0 \\ \cos\phi & 0 & \sin\phi \\ 0 & \sin\phi & 0 \end{bmatrix}, \quad (3a)$$

$$\hat{\Sigma}_y^{(3)}(\phi) = i\begin{bmatrix} 0 & -\cos\phi & 0 \\ \cos\phi & 0 & -\sin\phi \\ 0 & \sin\phi & 0 \end{bmatrix}. \quad (3b)$$

Moreover, $\nabla_\tau = \{\tau \partial/\partial x, \ \partial/\partial y\}$, and a 3×3 unit matrix $\hat{\Sigma}_0^{(3)}$ introduced in Eq. (2) is given by

$$\hat{\Sigma}_0^{(3)} = \begin{bmatrix} 1 & 0 & 0 \\ 0 & 1 & 0 \\ 0 & 0 & 1 \end{bmatrix}, \tag{4}$$

which is independent of phase ϕ. Specifically, for a dice lattice with $\phi = \pi/4$, the matrices in Eqs. (3) and (3b) are simplified to well-known 3×3 Pauli matrices, i.e.,

$$\hat{\Sigma}_x^{(3)} = \frac{1}{\sqrt{2}} \begin{bmatrix} 0 & 1 & 0 \\ 1 & 0 & 1 \\ 0 & 1 & 0 \end{bmatrix}, \tag{5a}$$

$$\hat{\Sigma}_y^{(3)} = \frac{i}{\sqrt{2}} \begin{bmatrix} 0 & -1 & 0 \\ 1 & 0 & -1 \\ 0 & 1 & 0 \end{bmatrix}. \tag{5b}$$

Additionally, in the presence of a finite band gap, the third Pauli matrix

$$\hat{\Sigma}_z^{(3)} = \begin{bmatrix} 1 & 0 & 0 \\ 0 & 0 & 0 \\ 0 & 0 & -1 \end{bmatrix}, \tag{6}$$

should be utilized in a Hamiltonian [88,89]. Here, the energy eigenvalues for the Hamiltonian in Eq. (1) are found to be

$$\varepsilon_{\tau,\phi}^{\gamma=\pm1}(\boldsymbol{k}) = \gamma \hbar v_F k, \tag{7}$$

where $\gamma = -1$ ($\gamma = +1$) corresponds to the valance (conduction) band, while $\gamma = 0$ leads to a dispersionless solution, given by

$$\varepsilon_{\tau,\phi}^{\gamma=0}(\boldsymbol{k}) = 0, \tag{8}$$

which is also known as a "flat band." Clearly, all three bands in Eqs. (7) and (8) are independent of phase ϕ (or parameter α). Furthermore, the wave functions corresponding to the valence and conduction bands in Eq. (7) are calculated as

$$\Psi_{\tau,\phi}^{\gamma=\pm1}(\boldsymbol{k}) = \frac{1}{\sqrt{2}} \begin{bmatrix} \tau \cos\phi \ e^{-i\tau\theta_{\mathbf{k}}} \\ \gamma \\ \tau \sin\phi \ e^{+i\tau\theta_{\mathbf{k}}} \end{bmatrix}, \tag{9}$$

where $\theta_{\mathbf{k}} = \arctan(k_y/k_x)$ is the angle of wave vector $\boldsymbol{k} = \{k_x, k_y\}$ made with the x-axis. The remaining wave function

attributed to the flat band takes the form

$$\Psi_{\tau,\phi}^{\gamma=0}(\boldsymbol{k}) = \begin{bmatrix} \sin\phi \ e^{-i\tau\theta_{\mathbf{k}}} \\ 0 \\ -\cos\phi \ e^{+i\tau\theta_{\mathbf{k}}} \end{bmatrix}. \tag{10}$$

Here, we would like to emphasize that the energy bands in Eqs. (7) and (8), as well as the wave functions in Eqs. (9) and (10), are obtained only for a spatially uniform potential independent of position coordinates x and y.

Specifically, for a dice lattice, we can set $\phi = \pi/4$ and the wave functions in Eqs. (9) and (10) become

$$\Psi_{\tau,\phi=\pi/4}^{\gamma=\pm1}(\boldsymbol{k}) = \frac{1}{2} \begin{bmatrix} e^{-i\tau\theta_{\mathbf{k}}} \\ \sqrt{2}\tau\gamma \\ e^{+i\tau\theta_{\mathbf{k}}} \end{bmatrix}, \tag{11a}$$

$$\Psi_{\tau,\phi=\pi/4}^{\gamma=0}(\boldsymbol{k}) = \frac{1}{\sqrt{2}} \begin{bmatrix} e^{-i\tau\theta_{\mathbf{k}}} \\ 0 \\ -e^{+i\tau\theta_{\mathbf{k}}} \end{bmatrix}, \tag{11b}$$

in which the top and bottom rows acquire the same magnitude.

III. SEMICLASSICAL WKB MODEL AND SOLUTION

In this section, our goal is to derive the so-called transport equations connecting different orders of the series expansion of the WKB wave function in powers of $\hbar$. This is a set of the most important differential equations which allow for the calculation of wave functions with unlimited precision. The most crucial one is the principal zero-order wave function ψ_0 which requires knowledge of the semiclassical action obtained from spatial derivative of the position-dependent longitudinal momentum of targeted electrons. In addition, we provide general solutions to the transport equations, calculate the next (first-order) term ψ_1 in the expansion of electron wave functions, and verify the convergence requirement $\psi_1 \ll \psi_0$ to ensure the accuracy of the WKB approximation. This is the major part of this paper including our most crucial findings.

A. WKB transport equation and action

We begin by applying our model to an electron moving in an x-dependent potential $V(x)$ such that its longitudinal momentum $p_x(x)$ also varies as a function of x. For this case, the wave function can be formally written as $\Psi(x, y) \backsim \psi(x) e^{ik_y y}$ due to the fact that the translational symmetry of the electron is maintained along the y direction. Therefore, the Hamiltonian in Eq. (2) becomes explicitly

$$\hat{\mathcal{H}}(x, k_y | \tau) = \begin{bmatrix} V(x) & v_F \cos\phi \, \Xi_\tau^-(x) & 0 \\ v_F \cos\phi \, \Xi_\tau^+(x) & V(x) & v_F \sin\phi \, \Xi_\tau^-(x) \\ 0 & v_F \sin\phi \, \Xi_\tau^+(x) & V(x) \end{bmatrix}, \tag{12a}$$

$$\Xi_\tau^\pm(x) = -i\hbar\tau \frac{\partial}{\partial x} \pm ip_y, \tag{12b}$$

which incorporate the translational symmetry of the system in the y direction, and we adopted the notation $p_y = \hbar k_y$ in Eq. (12b). The graphic description of this system is illustrated in Fig. 1. For a fixed incident energy E_γ of electrons,

as the potential energy $V(x)$ increases, electron longitudinal momentum $p_x(x)$ will eventually reduce to zero at some points called "turning points." Physically, these points specify a set of classically forbidding regions in which electrons acquire an
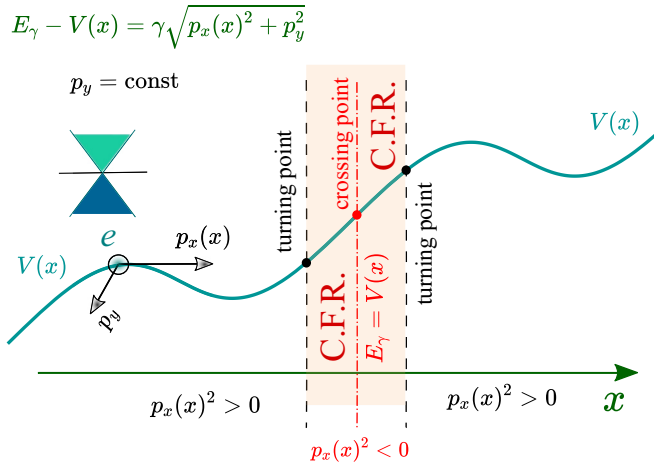
FIG. 1. Schematics for a Dirac electron moving with kinetic energy E_γ under a nonuniform potential $V(x)$, where the longitudinal momentum $p_x(x)$ of this electron will depend on its position x whereas the transverse momentum $p_y = \hbar k_y$ remains unchanged during its tunneling process. Meanwhile, we define a classically forbidden or classically inaccessible region by $p_x^2(x) < 0$ with its two boundaries known as turning points. Here, these crossing points are determined by the locations at which the condition $V(x) = E_\gamma$ is satisfied so that the transition between electron and hole states can occur.

imaginary longitudinal momentum due to $p_x^2(x) < 0$. Moreover, points satisfying $E_\gamma = V(x)$ appear as crossing ones between electron and hole states. In contrast to graphene, electron momentum at these points in α-$\mathcal{T}_3$ cannot be determined uniquely due to its infinite degeneracy of kinetic energy resulting from $E_\gamma - V(x) = 0$.

Emphasizing that we introduce an expansion approximation and estimate each of the terms in a series, it is important that we rewrite our initial eigenvalue equation in

dimensionless form. A similar approach was used previously in Refs. [4,5]. For this purpose, we will scale the energy in Eqs. (12) and (12b) by V_0, or simply $E \longrightarrow E/V_0$ and $V(x) \longrightarrow V(x)/V_0$. Here, the positive number V_0 could be taken as the maximum value of the potential $V(x)$. On the other hand, the length can be scaled by the barrier width W_B, or $x \longrightarrow x/W_B$. Correspondingly, the momentum should be scaled as $p_{x,y} \longrightarrow v_y p_{x,y}/V_0$, and most importantly, our (small) expansion parameter (i.e., Planck's constant) is modified according to

$$\hbar \longrightarrow \left(\frac{v_F}{W_B V_0} \right) \hbar, \tag{13}$$

and the spatial derivative would become $\partial/\partial x \to W_B \, \partial/\partial x$. Here, we avoid expressing the energy unit by the inverse length because this would introduce an additional term depending on a small parameter $\hbar$. Additionally, the incoming particles are assumed to be quasiclassical, i.e., they have a much larger kinetic energy than the Fermi energy of the system.

After performing all these scaling processes, the main eigenvalue equation can be rewritten as

$$\hat{\mathcal{H}}(x, p_y|\phi, \tau)\Psi^\gamma(x, p_y|\phi, \tau) = E_\gamma \Psi^\gamma(x, p_y|\phi, \tau), \tag{14}$$

where the wave function $\Psi^\gamma(x, p_y \,|\, \phi, \tau)$ takes the form

$$\Psi^\gamma(x, p_y|\phi, \tau) = \psi^\gamma(x|\phi, \tau)\exp\left(\frac{i}{\hbar} p_y y \right)$$

$$= \begin{bmatrix} \phi_A(x|\phi, \tau) \\ \phi_H(x) \\ \phi_B(x|\phi, \tau) \end{bmatrix} \exp\left(\frac{i}{\hbar} p_y y \right). \tag{15}$$

Correspondingly, the Hamiltonian presented in Eq. (14) becomes

$$\hat{\mathcal{H}}(x, p_y|\phi, \tau) = \hat{\Sigma}_0^{(3)} V(x) + \hat{\Sigma}_x^{(3)}(\phi)\left[-i\hbar\tau \frac{\partial}{\partial x} \right] + \hat{\Sigma}_y^{(3)}(\phi)p_y$$

$$= \begin{bmatrix} V(x) & v_F\, \Xi_\tau^-(x)\cos\phi & 0 \\ v_F\, \Xi_\tau^+(x)\cos\phi & V(x) & v_F\, \Xi_\tau^-(x)\sin\phi \\ 0 & v_F\, \Xi_\tau^+(x)\sin\phi & V(x) \end{bmatrix}. \tag{16}$$

A standard Wentzel-Kramers-Brillouin semiclassical approach is accomplished by expanding the unknown wave function in Eq. (15) as a series in powers of $\hbar$, yielding

$$\Psi(x, p_y|\phi, \tau) = \exp\left\{ \frac{i}{\hbar} \mathbb{S}(x, p_y|\phi, \tau) \right\} \sum_{\lambda=0}^\infty (-i\hbar)^\lambda \Psi_\lambda(x, p_y|\phi, \tau)$$

$$= \exp\left\{ \frac{i}{\hbar} \mathbb{S}(x, p_y|\phi, \tau) \right\} [\Psi_0(x, p_y|\phi, \tau) - i\hbar\Psi_1(x, p_y|\phi, \tau) - \hbar^2\Psi_2(x, p_y|\phi, \tau) + \cdots], \tag{17}$$

where $\mathbb{S}(x, p_y \,|\, \phi, \tau)$ represents a semiclassical action to be calculated. The issue for constructing a semiclassical approximation under an x-dependent potential can be resolved once we compute the WKB wave functions, or equivalently, all expansion terms in Eq. (17). Mathematically, we will derive a set of differential equations which connect all consecutive expansion terms in Eq. (17). These equations, referred to as the WKB *transport equations*, are key players in any semiclassical theory.

After a lengthy calculation, the transport equation for α-$\mathcal{T}_3$ is finally found to be

$$\hat{\Sigma}_x^{(3)}(\phi)\left\{ \frac{\partial}{\partial x} \Psi_\lambda(x, p_y|\phi, \tau) \right\} - \frac{1}{\sqrt{2}} \hat{\mathbb{O}}_T(x, p_y|\phi, \tau)\Psi_{\lambda+1}(x, p_y|\phi, \tau) = 0, \tag{18}$$

where $\lambda = 0, 1, 2, 3, \ldots$, and

$$\Psi_{\lambda<0}(x, p_y | \phi, \tau) \equiv 0. \tag{19}$$

In Eq. (18), the transport operator $\hat{\mathbb{O}}_T(x, p_y | \phi, \tau)$ which connects subsequent expansion terms in Eq. (17) is calculated as

$$\hat{\mathbb{O}}_T(x, p_y | \phi, \tau) = \begin{bmatrix} \nu(x) & \Xi_{\mathbb{S},\tau}^{(-)}(x, p_y) \cos\phi & 0 \\ \Xi_{\mathbb{S},\tau}^{(+)}(x, p_y) \cos\phi & \nu(x) & \Xi_{\mathbb{S},\tau}^{(-)}(x, p_y) \sin\phi \\ 0 & \Xi_{\mathbb{S},\tau}^{(+)}(x, p_y) \sin\phi & \nu(x) \end{bmatrix}, \tag{20}$$

where we introduce the notations, given by

$$\Xi_{\mathbb{S},\tau}^{(\pm)}(x, p_y) = \tau \frac{\partial \mathbb{S}(x)}{\partial x} \pm i p_y, \tag{21a}$$

$$\nu(x) = V(x) - E_\gamma. \tag{21b}$$

As an example, setting $\lambda = -1$ in Eq. (18), we obtain a simplified equation for the zeroth-order wave function

$$\hat{\mathbb{O}}_T(x, p_y | \phi, \tau)\Psi_0(x, p_y | \phi, \tau) = 0, \tag{22}$$

which constitutes a linear and homogeneous algebraic system. A nontrivial solution for such a system becomes possible only when its determinant equals zero, leading to the following equation:

$$-[E_\gamma - V(x)]\left\{ \left(\frac{\partial \mathbb{S}(x)}{\partial x} \right)^2 + p_y^2 - [E_\gamma - V(x)]^2 \right\} = 0, \tag{23}$$

which is independent of ϕ. We know that for a nonuniform potential $V(x)$, the condition $E_\gamma = V(x)$ will not always be fulfilled except at a finite number of turning points. Therefore, the classical action $\mathbb{S}(x)$ is calculated as

$$\mathbb{S}(x) = \mathbb{S}(x_0) + \int_{x_0}^x d\eta \, p_x(\eta), \tag{24a}$$

$$p_x(x | p_y) = \pm\sqrt{[E_\gamma - V(x)]^2 - p_y^2}, \tag{24b}$$

which is expressed through a position-dependent longitudinal momentum $p_x(x)$. However, the transverse momentum p_y remains the same due to the presence of a translational symmetry of the system and then can be treated as a given parameter.

B. Leading-order wave function

The key step in constructing a semiclassical approximation is calculating the leading-order (zero-order) electron wave function $\Psi_0(x | \phi, \tau)$ which has the following form:

$$\Psi_0(x | \phi, \tau) = \begin{bmatrix} \varphi_A^{(0)}(x | \phi, \tau) \\ \varphi_H^{(0)}(x | \phi, \tau) \\ \varphi_B^{(0)}(x | \phi, \tau) \end{bmatrix}. \tag{25}$$

Equations (20), (21a), (21b), (24a), and (24b) lead to the following wave function:

$$\Psi_0(x | \phi, \tau) = \begin{bmatrix} \cos\phi \, \Theta(x | \tau) \\ -1 \\ \sin\phi \, \Theta^\star(x | \tau) \end{bmatrix} \varphi_H^{(0)}(x | \phi, \tau), \tag{26a}$$

where the phase of wave function (26a) is given as

$$\Theta(x | \tau) = \frac{1}{\nu(x)}[\tau p_x(x) - i p_y] = -\tau \exp[-i\tau \theta_{\mathbf{p}}(x)]. \tag{27}$$

Also, $\Theta^\star(x | \tau) \overset{i \to -i}{\Longrightarrow} \Theta(x | \tau)$, $p_x^2(x) + p_y^2 \equiv \nu^2(x)$, while $\theta_{\mathbf{p}}(x) = \tan^{-1}[p_y/p_x(x)]$ is associated with the wave vector $\mathbf{p} = \{p_x(x), p_y\}$ depending on the position x, i.e., varies with the potential profile $V(x)$. Here, the x-dependent function $\varphi_H^{(0)}(x | \phi, \tau)$ in Eq. (26a) still remains unidentified at this moment, and we will determine it later from the general transport equation in Eq. (18).

We connect the known zeroth-order wave function $\Psi_0(x, p_y | \phi, \tau)$ with the unknown first-order one $\Psi_1(x, p_y | \phi, \tau)$ by setting $\lambda = 0$ in Eq. (18), giving rise to

$$\hat{\mathbb{O}}_T(x, p_y | \phi, \tau)\Psi_1(x, p_y | \phi, \tau)$$
$$= \sqrt{2}\hat{\Sigma}_x^{(3)}(\phi) \frac{\partial}{\partial x} \Psi_0(x, p_y | \phi, \tau). \tag{28}$$

The detailed derivation of zero-order wave function $\varphi_H^{(0)}(x | \phi)$ is given in Appendix A. Finally, it is calculated as

$$\varphi_H^{(0)}(x | \phi) = -\sqrt{\frac{p_x(x) + i p_y}{p_x(x)}} + \frac{i}{2} \sin^2\phi \tan^{-1}\left[-\frac{i p_x(x)}{p_y} \right], \tag{29}$$

which becomes independent of τ. We also point out that $\varphi_H^{(0)}(x | \phi)$ in Eq. (29) is valid up to a normalization constant as well as a phase factor. Consequently, our result in Eq. (29) for gapless graphene with $\phi = 0$ can differ by a complex phase $p_x(x) \pm i p_y$ compared to that in Ref. [5].

Taking a dice lattice with $\phi = \pi/4$ as an example, we find

$$\varphi_H^{(0)}(x) = \left[\frac{p_x^2(x) + p_y^2}{p_x^2(x)} \right]^{1/4} = \left\{ 1 + \left[\frac{p_y}{p_x(x)} \right]^2 \right\}^{1/4}. \tag{30}$$

Up to this point, the leading-order wave function $\Psi_0(x | \phi, \tau)$ in Eq. (26a) has been fully determined, including both the phase difference and spatial dependence of all three spinor components. Apart from that, all successive orders of the wave functions in the expansion in Eq. (17) could be determined by using the transport equation in Eq. (18), as we will do below for the first-order one $\Psi_1(x | \phi, \tau)$. One also notices that $\varphi_H^{(0)}(x)$ in Eq. (30) becomes divergent at the point where $p_x(x) = 0$, implying that the WKB approximation becomes invalid around a turning point, as seen from Fig. 1. The same situation was also predicted earlier for the case of graphene [5] and even a regular Schrödinger electron as well.

C. General solution for wave function

The general solution for the WKB wave-function transport is obviously obtained using the transport equation (18) for an arbitrary order λ written as

$$\frac{1}{\sqrt{2}}\hat{\mathbb{O}}_T(x, p_y|\phi, \tau)\Psi_\lambda(x, p_y|\phi, \tau)$$
$$- \hat{\Sigma}_x^{(3)}(\phi)\frac{\partial}{\partial x}\Psi_{\lambda-1}(x, p_y|\phi, \tau) = 0. \qquad (31)$$

The detailed derivation of the WKB wave function is provided in Appendix B. General transport equation (31) could be also obtained based in general results provided in Ref. [1]. In this paper, we mostly focus on the study of a dice lattice with $\phi = \pi/4$ which represents an independent practical interest.

From Eqs. (B3) to (B5), we obtain the following thee equations for the components of the wave function $\varphi_H^{[\lambda,(\pm,3)]}$:

$$- (\Theta + \Theta^\star)\left[\frac{d\varphi_H^{(\lambda-1,+)}}{dx} + \frac{d\varphi_H^{(\lambda-1,-)}}{dx}\right]$$
$$- \left[\frac{d\Theta^\star}{dx} + \frac{d\Theta}{dx}\right]\varphi_H^{(\lambda-1,+)}$$
$$- (\Theta - \Theta^\star)\frac{d\varphi_H^{(\lambda-1,3)}}{dx} + \left[\frac{d\Theta^\star}{dx} - \frac{d\Theta}{dx}\right]\varphi_H^{(\lambda-1,3)} = 0, \qquad (32)$$

as well as

$$(\Theta + \Theta^\star)\left[\frac{d\varphi_H^{(\lambda-1,+)}}{dx} - \frac{d\varphi_H^{(\lambda-1,-)}}{dx}\right]$$
$$+ \left[\frac{d\Theta^\star}{dx} + \frac{d\Theta}{dx}\right]\varphi_H^{(\lambda-1,+)}$$
$$+ (\Theta - \Theta^\star)\frac{d\varphi_H^{(\lambda-1,3)}}{dx} - \left[\frac{d\Theta^\star}{dx} - \frac{d\Theta}{dx}\right]\varphi_H^{(\lambda-1,3)}$$
$$= 4\sqrt{2}\nu(x)\varphi_H^{(\lambda,2)}, \qquad (33)$$

and, finally,

$$(\Theta - \Theta^\star)\frac{d\varphi_H^{(\lambda-1,-)}}{dx} = \sqrt{2}\nu(x)\varphi_H^{(\lambda,3)}. \qquad (34)$$

Here, $\Theta = \Theta(x|\tau)$ was given by Eq. (27). In $\phi_H^{\lambda,(1,2,3)}$ and $\phi_H^{\lambda-1,(\pm,3)}$, the index $\lambda = 0, 1, 2, \ldots$, stands for the order in a series expansion of wave function $\Psi_\lambda(x, p_y|\tau)$ in Eq. (18) so that the transport equation in Eq. (31) always connects two wave functions with successive orders of λ and $\lambda + 1$. The upper indices (1,2,3) label three expansion coefficients with respect to three orthogonal base vectors $|\mathbf{v}_1(x|\phi, \tau)\rangle$, $|\mathbf{v}_2(x|\phi, \tau)\rangle$ and $|\mathbf{v}_3(x|\phi, \tau)\rangle$. The lower index ϕ_H refers to the middle component of a wave-function column vector, corresponding to a hub hopping in $\alpha\text{-}T_3$ lattice. Finally, indices $\pm$ in wave functions $\phi_H^{\lambda,\pm}$ refer to two specific expressions $\phi_H^{\lambda,1}(x) \pm \phi_H^{\lambda,2}(x)$. As a whole, $\phi_H^{\lambda,(1,2,3)}$ and $\phi_H^{\lambda-1,(\pm,3)}$ correspond, respectively, to all these three configurations of wave functions.

Equations (32) to (34) can be employed to obtain three spinor components of each subsequent order wave function

$\varphi_H^{(\lambda,(1,2,3))}$ from the previous-order ones $\varphi_H^{(\lambda-1,(1,2,3))}$ in a general expansion in Eq. (17). Therefore, the issue for obtaining all orders of a WKB semiclassical wave function can be fulfilled. This constitutes one of the main efforts of this work.

D. First-order wave function and applicability of WKB approximation

Using the first-order transport equation

$$\hat{\mathbb{O}}_T(x, p_y|\phi, \tau)\Psi_1(x, p_y|\phi, \tau)$$
$$= \sqrt{2}\hat{\Sigma}_x^{(3)}(\phi)\frac{\partial}{\partial x}\Psi_0(x, p_y|\phi, \tau), \qquad (35)$$

where $\Psi_0(x, p_y|\phi, \tau) = \varphi_H^{(0)}(x|\phi, \tau)\,\mathbf{v}_1(x|\phi, \tau)$, we find a differential equation for determine $\varphi_H^{(0)}(x)$, given by

$$\varphi_H^{(0)}(x)\left[\frac{d\Theta^\star(x)}{dx} + \frac{d\Theta(x)}{dx}\right] + 2[\Theta^\star(x) + \Theta(x)]\frac{d\varphi_H^{(0)}(x)}{dx}$$
$$= 0, \qquad (36)$$

which is equivalent to Eq. (A11) and allow us to solve for the zeroth-order wave function $\varphi_H^{(0)}(x)$. The other two terms in Eq. (B2b) for the first-order wave function $\Psi_1(x, p_y|\phi, \tau)$ can be found directly from

$$\nu(x)\varphi_H^{(1,2)}(x) = \varphi_H^{(0)}(x)\frac{\sqrt{2}}{8}\left[\frac{d\Theta^\star(x)}{dx} + \frac{d\Theta(x)}{dx}\right], \qquad (37a)$$

$$\nu(x)\varphi_H^{(1,3)}(x) = \frac{\sqrt{2}}{2}[\Theta^\star(x) - \Theta(x)]\frac{d\varphi_H^{(0)}(x)}{dx}. \qquad (37b)$$

Finally, the most important differential equation to find the remaining term $\varphi_H^{(1,1)}(x)$ from $\varphi_H^{(1,2)}(x)$ and $\varphi_H^{(1,3)}(x)$ calculated from Eqs. (37a) and (37b) takes the form

$$2\Theta^+\frac{d\varphi_H^{(1,1)}}{dx} + \frac{d\Theta^+}{dx}\varphi_H^{(1,1)} = -\frac{d\Theta^+}{dx}\varphi_H^{(1,2)} + \frac{d\Theta^-}{dx}\varphi_H^{(1,3)}$$
$$+ \Theta^-\frac{d\varphi_H^{(1,3)}}{dx}, \qquad (38)$$

where $\Theta^\pm(x) = \Theta^\star(x) \pm \Theta(x)$.

By employing the Lagrange multiplier $\mu(x) = \exp[\int dx\, f(x)]$, we can immediately solve Eq. (38) and get

$$\varphi_H^{(1,1)}(x) = \exp\left[-\int^x d\xi\, f(\xi)\right]$$
$$\times \left\{\text{const} - \int^x d\xi\, g(\xi)\exp\left[\int^\xi d\eta\, f(\eta)\right]\right\},$$
$$f(x) = \frac{1}{2\Theta^+}\frac{d\Theta^+(x)}{dx},$$
$$g(x) = \frac{1}{2\Theta^+}\left[\varphi_H^{(1,2)}\frac{d\Theta^+}{dx} - \varphi_H^{(1,3)}\frac{d\Theta^-}{dx} - \Theta^-\frac{d\varphi_H^{(1,3)}}{dx}\right]. \qquad (39)$$

Equations (37a), (37b), and (39) together allow us to fully determining the first-order wave function $\Psi_1(x, p_y|\phi, \tau)$ for $\alpha\text{-}\mathcal{T}_3$ model based on the WKB approximation.

Since all the wave function terms up to the first order are found, we now turn to verifying the applicability of the WKB approximation, i.e., the magnitude of each subsequent-order term of the expansion in Eq. (17) is much smaller compared to the previous-order term, or $|\Psi_1(x)| \ll |\Psi_0(x)|$, and so on. For this purpose, let us first analyze Eq. (37a), which relates $\varphi_H^{(1,2)}(x)$ to $\varphi_H^{(0)}(x)$, as an example. We consider the case for particles with a large longitudinal momentum $p_x(x) \gg p_y$ and then turn to $p_x(x) \approx \nu(x)$. For Dirac cone particles, this corresponds to either a high potential energy $V(x)$ or a large initial kinetic energy E_γ of incoming electrons. In this situation, we are able to make use of the following approximations:

$$|\Theta^\star(x) + \Theta(x)| = \frac{2p_x(x)}{\nu(x)} \sim 1, \qquad (40a)$$

$$\frac{d}{dx}|\Theta^\star(x) + \Theta(x)| \approx \frac{p_y}{p_x^2(x)}\frac{dp_x(x)}{dx}. \qquad (40b)$$

Finally, the first-order term $\varphi_H^{(1,2)}(x)$ is estimated as

$$\begin{aligned}
\varphi_H^{(1,2)}(x) &= \frac{\sqrt{2}}{8}\frac{1}{\nu(x)}\left[\frac{d\Theta^\star(x)}{dx} + \frac{d\Theta(x)}{dx}\right]\varphi_H^{(0)}(x) \\
&\approx \frac{p_y}{p_x^2(x)\nu(x)}\frac{dp_x(x)}{dx}\varphi_H^{(0)}(x) \\
&\approx \left[\frac{p_y}{p_x^3(x)}\right]\varphi_H^{(0)}(x)\frac{dp_x(x)}{dx} \\
&= \left[\frac{p_y}{p_x(x)}\right]\left|\frac{d\lambda(x)}{dx}\right|\varphi_H^{(0)}(x),
\end{aligned} \qquad (41)$$

and its derivative

$$\left|\frac{d\lambda(x)}{dx}\right| \equiv \left|\frac{d}{dx}\left[\frac{\hbar}{p_x(x)}\right]\right| = \left[\frac{\hbar}{p_x^2(x)}\right]\left|\frac{dp_x(x)}{dx}\right|.$$

Thus, we obtain a standard criteria for the applicability of a semiclassical WKB approximation in quantum mechanics for a spatially slowly varying wavelength $\lambda(x)$ of incoming particles assisted by the condition $p_x(x) \gg p_y$ discussed above.

IV. APPLICATIONS OF WKB APPROXIMATION

The calculated successive-order wave functions can be applied to studying many physics problems, such as electron bound states and quantum tunneling, including α-decay and electron scattering. In this section, we present a brief discussion on how one can make use of the computed approximate semiclassical wave function for analyzing various tunneling properties of electrons in α-$\mathcal{T}_3$ material. From the physics perspective, the major application of a semiclassical theory aims at finding electron transmission for a nontrivial potential profile where a direct calculation of the transmission amplitude based on the Schrödinger equation becomes either impossible or too tedious, as well as studying resonant tunneling or scattering of an incident particle subjected to an electron-hole transition within a barrier region.

If we only know the action $\mathbb{S}(x)$, which directly relates to the x-dependent longitudinal momentum by $p_x(x) = \partial\mathbb{S}(x)/\partial x$, then it is sufficient to estimate the electron transmission $T(p_y \,|\, \{\nu(x)\}, \phi)$ through any potential barrier $V(x)$ as an integral of $p_x(x)$, given by

$$\begin{aligned}
&T(p_y | \{\nu(x)\}, \phi, \Delta_0) \\
&= \exp\left(-\frac{2}{\hbar}\int_{\text{CFR}}dx|p_x(x|p_y, \phi, \Delta_0)|\right), \qquad (42)
\end{aligned}$$

where the integration will be performed only over the so-called classically forbidden regions (CFR) corresponding to $p_x^2(x) < 0$, i.e., $p_x(x)$ becomes purely imaginary [8,9]. Such nonclassical states of a particle lead to a significant decrease of the transmission coefficient in Eq. (42). According to Eq. (42), the area under the curve $\text{Im}[p_x(x \,|\, k_y, \phi, \Delta_0)]$ characterizes the exponential suppression of electron tunneling by the presence of CFR's, where both the magnitude and spatial span of CFR's will play a crucial role.

To quantify the characteristics of CFR's, let us consider an α-$\mathcal{T}_3$ material with a finite energy band gap Δ. Technically, the condition $\Delta > 0$ could be satisfied either by using a dielectric substrate or irradiating our sample with an external off-resonance dressing optical field [31,88]. By including this finite band gap Δ, the gap-correction term $\hat{\mathcal{H}}_\Delta(\phi)$ to the previous Hamiltonian in Eq. (2) for a gapless α-$\mathcal{T}_3$ lattice can be constructed by directly adding a ϕ-dependent $\hat{\Sigma}_z(\phi)$ term, leading to

$$\hat{\mathcal{H}}_\Delta(\phi) = \frac{\Delta_0}{2}\hat{\Sigma}_z(\phi) = \Delta_0\begin{bmatrix} \cos^2\phi & 0 & 0 \\ 0 & -\cos 2\phi & 0 \\ 0 & 0 & -\sin^2\phi \end{bmatrix}, \quad \hat{\Sigma}_z(\phi) = -i[\hat{\Sigma}_x(\phi), \hat{\Sigma}_y(\phi)]_-, \qquad (43)$$

as it was derived in Ref. [63]. After having included $\hat{\mathcal{H}}_\Delta(\phi)$ in Eq. (43), the previous transport operator $\hat{\mathbb{O}}_T(x, p_y | \phi, \tau)$ in Eq. (20) should be modified as

$$\hat{\mathbb{O}}_T(x, p_y, \Delta_0 | \phi, \tau) = \begin{bmatrix} \nu(x) + \Delta_0\cos^2\phi & \cos\phi\,\Xi(x)_{\mathbb{S},\tau}^- & 0 \\ \cos\phi\,\Xi(x)_{\mathbb{S},\tau}^+ & \nu(x) - \Delta_0\cos^2\phi & \sin\phi\,\Xi(x)_{\mathbb{S},\tau}^- \\ 0 & \sin\phi\,\Xi(x)_{\mathbb{S},\tau}^+ & \nu(x) - \Delta_0\sin^2\phi \end{bmatrix}, \quad \Xi(x)_{\mathbb{S},\tau}^\pm = -i\hbar\tau\frac{\partial\mathbb{S}_\Delta(x)}{\partial x} \pm ip_y, \qquad (44)$$

where $\Delta_0 = \Delta/V_0$ with V_0 being the height of a constant potential. The longitudinal momentum $p_x(x \,|\, \Delta_0, \phi)$ in Eq. (24b) now takes the new form

$$[p_x(x|\Delta_0, \phi)]^2 = \nu^2(x) - p_y^2 + \frac{\Delta_0^2}{8\nu(x)}\sin(2\phi)\sin(4\phi) - \frac{\Delta_0^2}{8}[5 + 3\cos(4\phi)]. \qquad (45)$$
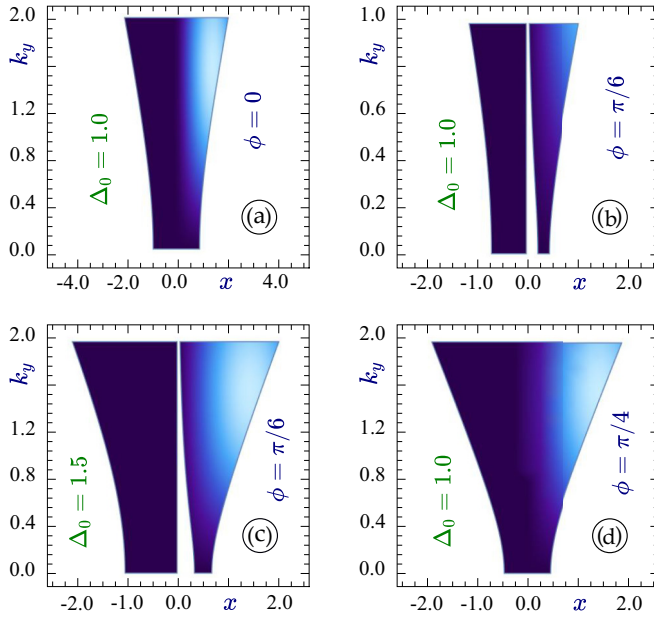
FIG. 2. Calculated two-dimensional (2D) density plots for classically forbidden regions (CFR's) $|\text{Im}[p_x(x \,|\, k_y, \phi, \Delta_0)]|$ as functions of both position x and transverse wave number k_y of an electron in gapped α-$\mathcal{T}_3$ materials with various values of band gap Δ_0 and geometry phase ϕ. Here, the electron moves under a linearly increasing potential $V(x) = V_0 + ax$, where $a = 1$ is set for all plots and $V_0 = E_\gamma$ is determined from the condition $v(x) = V(x) - E_\gamma = 0$ at $x = 0$. As labeled, three specific values of ϕ are selected for $\phi = 0$ (graphene), $\phi = \pi/6$, and $\phi = \pi/4$ (a dice lattice).

The CFR's calculated from Eq. (45) for gapped α-$\mathcal{T}_3$ are presented in Figs. 2–5 for a linear $V(x) = V_0 + ax$ and nonlinear $V(x) = V_0 + a\,\text{sign}(x)\,x^2$ potential profiles, where a represents a field parameter for generating the x dependence of the potential $V(x)$. From Figs. 2–5, we find a substantial difference between these two different types of potential, and such a difference will strongly affect the electron tunneling. Meanwhile, we also observe that the span of these CFR's generally decreases with increasing ϕ. It is important to point out that, for $0 < \phi < \pi/4$, there exists a pole determined by $v(x) = V(x) - E_\gamma = 0$ and the sign of the term $\Delta_0^2 \sin(2\phi) \sin(4\phi)/[8\,v(x)]$ would switch at this pole. This implies that $x = 0$ must always be one boundary of a CFR, as seen in all plots of Figs. 2–5 when $\Delta_0 \neq 0$ except for graphene ($\phi = 0$) and a dice lattice ($\phi = \pi/4$).

Additionally, E_γ represents the total energy of an incoming particle (an independent variable and a parameter in our computations) and is chosen as $E_\gamma = 1.0$ in units of electron Fermi energy $E_F^{(0)} = 50\,\text{meV}$. Here, $\gamma = 1$ means the particle energies above the band gap (or in a conduction band), while $\gamma = 0$ or -1 correspond to particles in a flat or a valence band, separately. Physically, the change of E_γ leads to a shift of the crossing point (where the particle energy is chosen to be zero and sits at $x = 0$ for all out plots).

As shown in Eq. (42), within the WKB-approximation frame, the electron transmission $T(p_y \,|\, \{v(x)\}, \Delta_0, \phi)$ relies only on the spatial distribution of a longitudinal momentum $p_x(x)$ within the CFR's. On the other hand, $p_x(x)$ can be uniquely determined through $p_x(x) = \sqrt{v^2(x) - p_y^2}$ for any
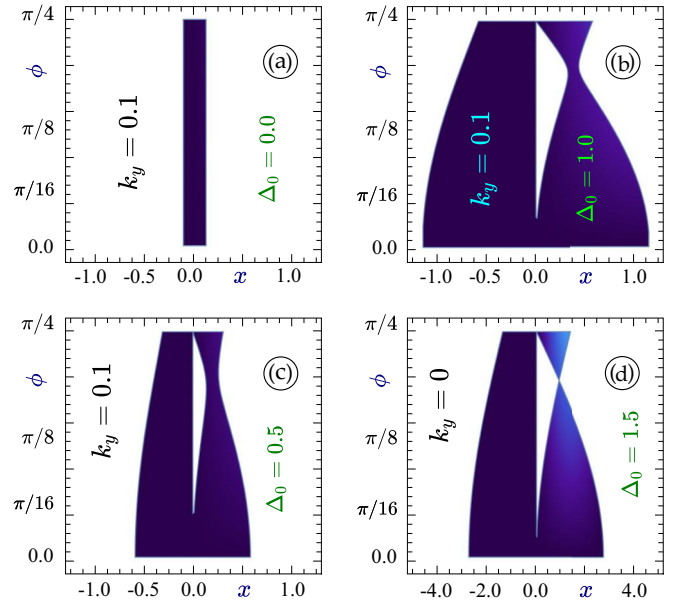
FIG. 3. Calculated 2D density plots for $|\text{Im}[p_x(x \,|\, k_y, \phi, \Delta_0)]|$ as functions of both x and ϕ of an electron in gapped α-$\mathcal{T}_3$ materials with various values of Δ_0 and k_y. Here, the electron moves under a potential $V(x) = V_0 + ax$ with $a = 1$ and $V_0 = E_\gamma$ for all plots. As indicated, the values of k_y are assumed to be $k_y = 0.1$ in panels (a)–(c) and $k_y = 0$ in plot (d).

assumed potential profile $v(x)$ and a given electron transverse momentum p_y. Therefore, $T(p_y \,|\, \{v(x)\}, \Delta_0, \phi)$ can be quantitatively controlled by the spatial dependence of CFR's in addition to other model parameters, such as the band gap
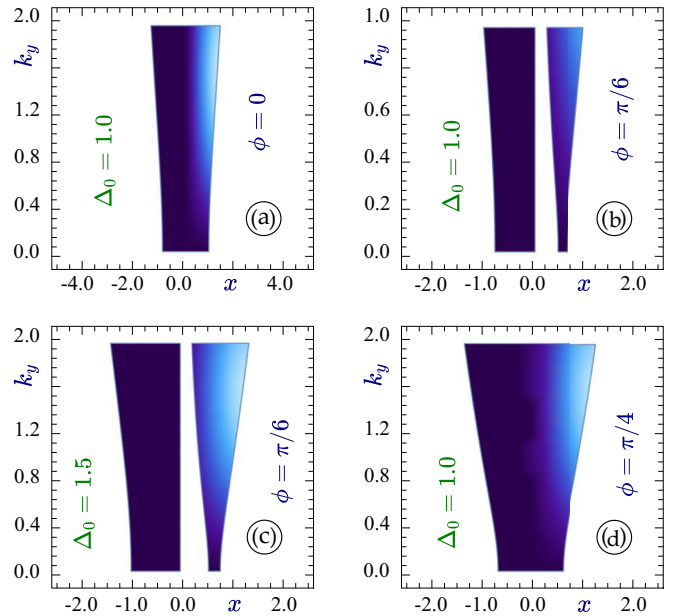
FIG. 4. Calculated 2D density plots for $|\text{Im}[p_x(x \,|\, k_y, \phi, \Delta_0)]|$ as functions of both x and k_y of an electron in gapped α-$\mathcal{T}_3$ materials with various values of Δ_0 and ϕ. Here, the electron moves under a potential $V(x) = V_0 + a\,\text{sign}(x)\,x^2$ with $a = 1$ and $V_0 = E_\gamma$ for all plots. The values of ϕ are taken as $\phi = 0$ (graphene), $\phi = \pi/6$, and $\phi = \pi/4$ (a dice lattice), as labeled.
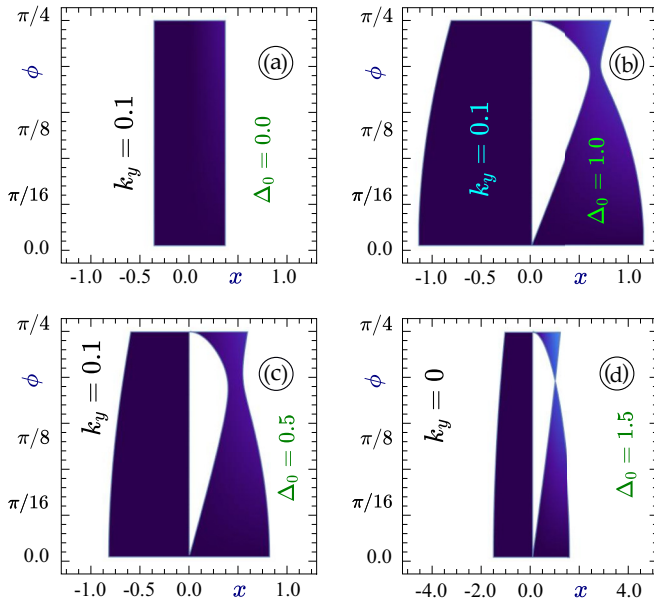
FIG. 5. Calculated 2D density plots for CFR's $|\text{Im}[p_x(x\,|\,k_y, \phi, \Delta_0)]|$ as functions of both x and ϕ of an electron in gapped $\alpha\text{-}\mathcal{T}_3$ materials with various values of Δ_0 and k_y. Here, the electron moves under a potential $V(x) = V_0 + a\,\text{sign}(x)\,x^2$ with $a = 1$ and $V_0 = E_\gamma$ for all plots. The values of k_y are selected as $k_y = 0.1$ for panels (a)–(c) and $k_y = 0$ for plot (d).

Δ_0 and the geometrical phase ϕ of $\alpha\text{-}\mathcal{T}_3$ lattices. Moreover, $T(p_y\,|\,\{v(x)\}, \Delta_0, \phi)$ will also depend on a given electron incident energy E_γ and transverse momentum p_y for assigned incident direction. Consequently, a thorough numerical study on the x dependence of CFR's and its relations to the parameters Δ_0, ϕ, and k_y become a main ingredient of the present paper, as discussed in detail below.

First, for a linear potential profile $V(x) = V_0 + a\,x$ employed in Fig. 2, we find that the span and magnitude of $|\text{Im}[p_x(x\,|\,k_y, \phi, \Delta_0)]|$ or the CFR in the $x > 0$ region is increased rapidly with k_y for $\phi = 0$ and $\pi/4$ in a symmetrical fan shape with respect to $x = 0$. But this increase of $|\text{Im}[p_x(x\,|\,k_y, \phi, \Delta_0)]|$ becomes asymmetrical in shape and splits around $x = 0$ for $\phi = \pi/6$, which is further accompanied by a significant enhancement both in its magnitude and extent simultaneously as Δ_0 is increased from 1.0 to 1.5.

Additionally, for the chosen $k_y = 0.1$, we deduce from Fig. 3 that a narrow strip-shape distribution of CFR is independent of ϕ as $\Delta_0 = 0$ for the gapless case. However, both the span and splitting of $|\text{Im}[p_x(x\,|\,k_y, \phi, \Delta_0)]|$ are clearly widened as Δ_0 is increased from 0.5 to 1.0. In addition, the splitting of the CFR around $x = 0$ only occurs for finite ϕ but the splitting is always closed again at $\phi = \pi/4$. As Δ_0 is further increased from 0.5 to 1.0, both the span and splitting of the CFR are expanded dramatically. Even if $k_y = 0$, the same broadening and splitting features of the CFR remain for $\Delta_0 = 1.5$, and the magnitude of the CFR is increased greatly at the same time in comparison with other situations discussed.

Next, for a nonlinear potential profile $V(x) = V_0 + a\,\text{sign}(x)\,x^2$ used in Fig. 4, we observe that both the span and magnitude of the CFR at $\Delta_0 = 1$ are increased rapidly with k_y

symmetrically as ϕ is changed from 0 to $\pi/4$. However, such a symmetrical increase of CFR turns into an asymmetrical one with respect to $x = 0$ as $\phi = \pi/6$. In addition, for $\phi = \pi/6$, the same CFR becomes split around $x = 0$, and meanwhile, it demonstrates significant enhancements both in its magnitude and span simultaneously as Δ_0 is changed from 1.0 to 1.5.

Additionally, for the chosen $k_y = 0.1$, we see from Fig. 5 that a strip-like CFR spatial distribution is found independent of ϕ for a gapless situation with $\Delta_0 = 0$. However, the span and splitting of $|\text{Im}[p_x(x\,|\,k_y, \phi, \Delta_0)]|$ are both enlarged as Δ_0 is changed from 0.5 to 1.0. Differently, the splitting of CFR around $x = 0$ occurs for all values of ϕ except for two points at $\phi = 0$ and $\pi/4$. As Δ_0 is further raised from 0.5 to 1.0, the span and splitting of CFR increase significantly. However, when $k_y = 0$ for normal incidence of a particle, both the span and splitting of the CFR are weakened sharply for $\Delta_0 = 1.5$, but the magnitude of the CFR is still increased noticeably compared with other addressed cases with $k_y = 0.1$. Similarly, for the case of a nonlinear potential profile, the splitting of the CFR exists for all values of ϕ, except for graphene with $\phi = 0$ and a dice lattice with $\pi/4$.

By comparing Fig. 2 with Fig. 4, we conclude that the span of $|\text{Im}[p_x(x\,|\,k_y, \phi, \Delta_0)]|$ for a nonlinear potential profile at large values of k_y has been significantly reduced in addition to the appearance of a widened gap which implies that the corresponding tunneling will be greatly enhanced for nonnormal incidence of an electron. On the other hand, from a direct comparison between Figs. 3 and 5, we further find that, due to an expanding span of $|\text{Im}[p_x(x\,|\,k_y, \phi, \Delta_0)]|$ at $\Delta_0 = 0$, the introduced nonlinearity to a potential profile will sharply suppress the electron tunneling for nonnormal incidence for the same geometrical phase ϕ of gapless $\alpha\text{-}\mathcal{T}_3$ materials.

V. CONCLUDING REMARKS AND SUMMARY

In summary, this paper embodies our effort to construct a complete semiclassical description for the $\alpha\text{-}\mathcal{T}_3$ model which characterizes a wide class of Dirac cone materials with an additional flat band in their energy dispersion, also referred to as pseudospin-1 Dirac materials. So far, there has been immense and strong experimental evidence for the existence of a flat energy band in a large number of laboratory-synthesized materials. Anyone of these materials can be described by the theoretical $\alpha\text{-}\mathcal{T}_3$ model with a certain degree of precision so that our results are expected to be relevant to many existing two-dimensional lattices.

Our development of the WKB approximation includes finding a semiclassical action specifically for the $\alpha\text{-}\mathcal{T}_3$ model, as well as for the position-dependent longitudinal momentum; calculating the leading (zeroth) order wave function, all of its spinor components, their phase differences and spatial distributions. Most importantly, we explicitly derived a complete set of transport equations which relate any two subsequent orders of semiclassical wave function, i.e., $\Psi_\lambda(x, p_y\,|\,\phi, \tau)$ and $\Psi_{\lambda+1}(x, p_y\,|\,\phi, \tau)$. Therefore, the sought WKB wave function could now be obtained up to any desired order and precision. As an example, we solved these transport equations for the first-order wave function and demonstrated conditions for the applicability of the WKB approximation to our model Hamiltonian, e.g., requested $\Psi_1(x, p_y\,|\,\phi, \tau) \ll \Psi_0(x, p_y\,|\,\phi, \tau)$. In

particular, our derivations and obtained results for α-$\mathcal{T}_3$ appear drastically different from the standard WKB approximation for a Schrödinger particle, as frequently discussed in quantum mechanics textbooks and previously known results for graphene [5].

Our derived equations and calculated semiclassical electronic states could be further applied to investigate most of crucial electronic properties of α-$\mathcal{T}_3$ materials. Also, we discussed possible applications of our computed wave function to studying tunneling and transport properties of pseudospin-1 Dirac electrons under nontrivial potential profiles. Specifically, we considered the case for gapped α-$\mathcal{T}_3$, for which the direct computation of the wave function becomes complicated and impossible if a spatially nonuniform potential is assumed. In this work, the calculation of electron transmission in these cases is fulfilled simply by integrating a longitudinal electron momentum $|p_x(x)|$ over the so-called classically forbidden regions satisfying $p_x^2(x) < 0$. Using this scheme, we computed the transmission for various kinds of α-$\mathcal{T}_3$ lattices and demonstrated that the transmission is significantly reduced for a large geometrical phase ϕ. Technically, our developed semiclassical theory for a pseudospin-1 Dirac electron could be employed to numerically explore resonant tunneling and scattering of electrons by a potential barrier, as well as to characterize possible trapped or localized electronic states in α-$\mathcal{T}_3$.

We are confident that our work will play an important role for investigating fundamental electronic properties of a wide range of innovative low-dimensional structures. Building up a WKB approximation has been regarded as a key step for numerically studying each newly discovered material or a model Hamiltonian. Our obtained results will undoubtedly find their applications in the follow-up research on electron tunneling and transport properties, electrical control of α-$\mathcal{T}_3$ materials, designing and fabricating electronic devices and transistors based on resonant tunneling or scattering of Dirac electrons through an assigned potential barrier profile. Our results are also expected to be important in valleytronic applications due to the fact that low-energy electronic states of gapped α-$\mathcal{T}_3$ materials directly rely on a valley index, as well as many other applications of these unique and innovative materials.

APPENDIX A: LEADING-ORDER WAVE FUNCTION

The leading-order or zeroth-order wave function $\Psi_0(x \,|\, \phi, \tau)$ has the following form:

$$\Psi_0(x|\phi,\tau) = \begin{bmatrix} \varphi_A^{(0)}(x|\phi,\tau) \\ \varphi_H^{(0)}(x|\phi,\tau) \\ \varphi_B^{(0)}(x|\phi,\tau) \end{bmatrix}. \tag{A1}$$

Then, by using Eqs. (20), (21a), (21b), (24a), and (24b), we find

$$v(x)\varphi_A^{(0)}(x) + \cos\phi[\tau p_x(x) - ip_y]\varphi_H^{(0)}(x) = 0, \tag{A2a}$$

$$\sin\phi[\tau p_x(x) + ip_y]\varphi_H^{(0)}(x) + v(x)\varphi_B^{(0)}(x) = 0, \tag{A2b}$$

which leads to the solution

$$\Psi_0(x|\phi,\tau) = \begin{bmatrix} \cos\phi\,\Theta(x|\tau) \\ -1 \\ \sin\phi\,\Theta^\star(x|\tau) \end{bmatrix} \varphi_H^{(0)}(x|\phi,\tau), \tag{A3a}$$

$$\Theta(x|\tau) = \frac{1}{v(x)}[\tau p_x(x) - ip_y]$$

$$= -\tau\exp[-i\tau\theta_\mathbf{p}(x)], \tag{A3b}$$

$$\Theta^\star(x|\tau) \overset{i\to -i}{\Longrightarrow} \Theta(x|\tau), \tag{A3c}$$

where $p_x^2(x) + p_y^2 \equiv v^2(x)$, while $\theta_\mathbf{p}(x) = \tan^{-1}[p_y/p_x(x)]$ is associated with the wave vector $\mathbf{p} = \{p_x(x), p_y\}$ depending on the position x, i.e., varies with the potential profile $V(x)$. Here, the x-dependent function $\varphi_H^{(0)}(x \,|\, \phi, \tau)$ in Eq. (26a) still remains unidentified at this moment and we will determine it later from the general transport equation in Eq. (18).

Next, we would connect the known zeroth-order wave function $\Psi_0(x, p_y \,|\, \phi, \tau)$ with the unknown first-order one $\Psi_1(x, p_y \,|\, \phi, \tau)$ by setting $\lambda = 0$ in Eq. (18), giving rise to

$$\hat{\mathbb{O}}_T(x, p_y|\phi,\tau)\Psi_1(x, p_y|\phi,\tau)$$

$$= \sqrt{2}\hat{\Sigma}_x^{(3)}(\phi)\frac{\partial}{\partial x}\Psi_0(x, p_y|\phi,\tau). \tag{A4}$$

Here, the undetermined wave function $\Psi_1(x, p_y \,|\, \phi, \tau)$, corresponding to a state vector in three-dimensional Hilbert space, could be decomposed into a linear combination of three orthonormal basis vectors denoted as $|\mathbf{v}_1\rangle$, $|\mathbf{v}_2\rangle$, and $|\mathbf{v}_3\rangle$.

The first basis vector $|\mathbf{v}_1\rangle$ is equivalent to the spinor part of $\Psi_0(x, p_y \,|\, \phi, \tau)$ in Eq. (26a), i.e.,

$$|\mathbf{v}_1(x|\phi,\tau)\rangle = \begin{bmatrix} \cos\phi\,\Theta(x|\tau) \\ -1 \\ \sin\phi\,\Theta^\star(x|\tau) \end{bmatrix}, \tag{A5}$$

which implies that $\hat{\mathbb{O}}_T(x, p_y \,|\, \phi, \tau)|\mathbf{v}_1\rangle = 0$ as a result of Eq. (22). Meanwhile, we simply choose two remaining orthonormal vectors $|\mathbf{v}_2(\xi \,|\, \phi, \tau)\rangle$ and $|\mathbf{v}_3(\xi \,|\, \phi, \tau)\rangle$ as follows:

$$|\mathbf{v}_2(x|\phi,\tau)\rangle = \begin{bmatrix} \cos\phi\,\Theta(x|\tau) \\ +1 \\ \sin\phi\,\Theta^\star(x|\tau) \end{bmatrix}, \tag{A6}$$

$$|\mathbf{v}_3(x|\phi,\tau)\rangle = \begin{bmatrix} \sin\phi\,\Theta(x|\tau) \\ 0 \\ -\cos\phi\,\Theta^\star(x|\tau) \end{bmatrix}. \tag{A7}$$

Consequently, the state vector $\Psi_1(x, p_y \,|\, \phi, \tau)$ can be expanded by $|\mathbf{v}_1\rangle$, $|\mathbf{v}_2\rangle$, and $|\mathbf{v}_3\rangle$, and written as

$$\Psi_1(x, p_y|\phi,\tau) = \varphi_H^{(0)}(x)|\mathbf{v}_1\rangle + \varphi_H^{(1,2)}(x)|\mathbf{v}_2\rangle$$

$$+ \varphi_H^{(1,3)}(x)|\mathbf{v}_3\rangle, \tag{A8}$$

where we made use of the fact that $\varphi_H^{(0)}(x)$ in Eq. (26a) represents the spinor-amplitude function of $\Psi_0(x, p_y \,|\, \phi, \tau)$.

Next, making use of the result in Eq. (A8), we obtain

$$\langle \boldsymbol{v}_1 | \hat{\mathbb{O}}_T(x, p_y | \phi, \tau) | \Psi_1(x, p_y | \phi, \tau) \rangle$$

$$= \langle \boldsymbol{v}_1 | \hat{\mathbb{O}}_T(x, p_y | \phi, \tau) | \{ | \varphi_H^{(0)}(x) | \boldsymbol{v}_1 \rangle$$

$$+ \varphi_H^{(1,2)}(x) | \boldsymbol{v}_2 \rangle + \varphi_H^{(1,3)}(x) | \boldsymbol{v}_3 \rangle \} \rangle = 0 \quad (A9)$$

since the transport operator $\hat{\mathbb{O}}_T(x, p_y | \phi, \tau)$ is Hermitian and $\hat{\mathbb{O}}_T(x, p_y | \phi, \tau) | \boldsymbol{v}_1 \rangle = 0$. Therefore, the first-order transport equation in Eq. (28) now reads

$$\langle \boldsymbol{v}_1 | \hat{\Sigma}_x^{(3)}(\phi) \frac{\partial}{\partial x} \Psi_0(x, p_y | \phi, \tau) \rangle$$

$$= \langle \boldsymbol{v}_1 | \hat{\Sigma}_x^{(3)}(\phi) \frac{\partial}{\partial x} \{ | \boldsymbol{v}_1 \rangle \varphi_H^{(0)}(x | \phi, \tau) \} \rangle = 0, \quad (A10)$$

or equivalently, it can be rewritten as

$$[\Theta(x|\tau) + \Theta^{\star}(x|\tau)] \frac{\partial \varphi_H^{(0)}(x|\phi, \tau)}{\partial x} + \Gamma_\alpha(x|\tau) \varphi_H^{(0)}(x|\phi, \tau)$$

$$= 0, \quad (A11)$$

where

$$\Gamma_\alpha(x|\tau) = \frac{\partial \Theta(x|\tau)}{\partial x} + \sin^2 \phi \frac{\partial}{\partial x} [\Theta^{\star}(x|\tau) - \Theta(x|\tau)]. \quad (A12)$$

Here, the ϕ-dependence in Eq. (A12) could be rewritten by using the relative hopping parameter α as $\sin^2 \phi = \alpha^2/(1 + \alpha^2)$. Also, it worth mentioning that for a dice lattice with $\phi = \pi/4$, the function $\Gamma_{\alpha=1}(x|\tau) = \partial/\partial x[\Theta(x|\tau) + \Theta^{\star}(x|\tau)]$ becomes fully symmetric with respect to the interchange $\Theta(x|\tau) \leftrightarrow \Theta^{\star}(x|\tau)$. For $\phi = 0$ in particular, we obtain the same equation as that for graphene in Ref. [5].

Mathematically, Eq. (A11) acquires a general solution, given by

$$\varphi_H^{(0)}(x|\phi, \tau)$$

$$= c_0 \exp \left\{ -\int^x [\Theta(\xi|\tau) + \Theta^{\star}(\xi|\tau)]^{-1} \Gamma_\alpha(\xi|\tau) d\xi \right\}. \quad (A13)$$

Explicitly, we evaluated the employed functions in Eqs. (A11) to (A13) as

$$\Theta(x|\tau) = \frac{p_{\tau,-}(x)}{v(x)} = -\frac{\tau p_x(x) - i p_y}{p(x)},$$

$$\Theta^{\star}(x|\tau) = \frac{p_{\tau,+}(x)}{v(x)} = -\frac{\tau p_x(x) + i p_y}{p},$$

$$\frac{1}{\Theta(x|\tau) + \Theta^{\star}(x|\tau)} = -\frac{\tau p(x)}{2 p_x(x)},$$

$$\frac{\partial \Theta(x|\tau)}{\partial x} = -\frac{i \tau p_y}{p_{\tau,+}^{3/2}(x) p_{\tau,-}^{1/2}(x)} \frac{\partial p_x(x)}{\partial x},$$

$$\frac{\partial \Theta(x|\tau)^{\star}}{\partial x} = \frac{i \tau p_y}{p_{\tau,+}^{1/2}(x) p_{\tau,-}^{3/2}(x)} \frac{\partial p_x(x)}{\partial x}, \quad (A14)$$

where $p(x) = \sqrt{p_x^2(x) + p_y^2}$. Using derived identities in Eq. (A14), Eq. (A13) is calculated as

$$\varphi_H^{(0)}(x|\phi) = -\sqrt{\frac{p_x(x) + i p_y}{p_x(x)}} + \frac{i}{2} \sin^2 \phi \tan^{-1} \left[-\frac{i p_x(x)}{p_y} \right], \quad (A15)$$

which becomes independent of τ. We also point out that $\varphi_H^{(0)}(x|\phi)$ in Eq. (29) is valid up to a normalization constant as well as a phase factor. Consequently, our result in Eq. (29) for gapless graphene with $\phi = 0$ can differ by a complex phase $p_x(x) \pm i p_y$ compared to that in Ref. [5].

Taking a dice lattice with $\phi = \pi/4$ as an example, we find

$$\varphi_H^{(0)}(x) = \left[\frac{p_x^2(x) + p_y^2}{p_x^2(x)} \right]^{1/4} = \left\{ 1 + \left[\frac{p_y}{p_x(x)} \right]^2 \right\}^{1/4}. \quad (A16)$$

Thus, we derived Eqs. (29) and (30).

APPENDIX B: GENERAL SOLUTION FOR WAVE FUNCTION

Let us start with the general transport equation in Eq. (18), written as

$$\frac{1}{\sqrt{2}} \hat{\mathbb{O}}_T(x, p_y | \phi, \tau) \Psi_\lambda(x, p_y | \phi, \tau)$$

$$- \hat{\Sigma}_x^{(3)}(\phi) \frac{\partial}{\partial x} \Psi_{\lambda-1}(x, p_y | \phi, \tau) = 0, \quad (B1)$$

Here, both wave functions $\Psi_{\lambda-1}(x, p_y | \phi, \tau)$ and $\Psi_\lambda(x, p_y | \phi, \tau)$ are assumed to be expended over an orthonormal basis state-vector set $|\boldsymbol{v}_1\rangle$, $|\boldsymbol{v}_2\rangle$, and $|\boldsymbol{v}_3\rangle$, given by

$$\Psi_{\lambda-1}(x, p_y | \phi, \tau) = \varphi_H^{(\lambda-1,1)}(x|\phi, \tau) | \boldsymbol{v}_1 \rangle + \varphi_H^{(\lambda-1,2)}(x|\phi, \tau) | \boldsymbol{v}_2 \rangle + \varphi_H^{(\lambda-1,3)}(x|\phi, \tau) | \boldsymbol{v}_3 \rangle, \quad (B2a)$$

$$\Psi_\lambda(x, p_y | \phi, \tau) = \varphi_H^{(\lambda,1)}(x|\phi, \tau) | \boldsymbol{v}_1 \rangle + \varphi_H^{(\lambda,2)}(x|\phi, \tau) | \boldsymbol{v}_2 \rangle + \varphi_H^{(\lambda,3)}(x|\phi, \tau) | \boldsymbol{v}_3 \rangle . \quad (B2b)$$

By multiplying each side of Eq. (31) with $\langle \boldsymbol{v}_1 |$, $\langle \boldsymbol{v}_2 |$, and $\langle | \boldsymbol{v}_3 |$, respectively, it leads us to the following three coupled differential equations:

$$\left[(\Theta + \Theta^{\star}) \frac{d \varphi_H^{(\lambda-1,1)}}{dx} + (\varphi_H^{(\lambda-1,1)} + \varphi_H^{(\lambda-1,2)}) \frac{d\Theta}{dx} + (\Theta - \Theta^{\star}) \frac{d \varphi_H^{(\lambda-1,2)}}{dx} \right] \cos^2 \phi$$

$$- \left[\varphi_H^{(\lambda-1,3)} \left(\frac{d\Theta^{\star}}{dx} - \frac{d\Theta}{dx} \right) \varphi_H^{(\lambda-1,3)} + (\Theta^{\star} - \Theta) \frac{d \varphi_H^{(\lambda-1,3)}}{dx} \right] \frac{1}{2} \sin(2\phi)$$

$$+ \left[\frac{d\Theta^{\star}}{dx} \left(\varphi_H^{(\lambda-1,1)} + \varphi_H^{(\lambda-1,2)} \right) + \Theta \left(\frac{d\varphi_H^{(\lambda-1,1)}}{dx} - \frac{d\varphi_H^{(\lambda-1,2)}}{dx} \right) + \Theta^{\star} \left(\frac{d\varphi_H^{(\lambda-1,1)}}{dx} + \frac{d\varphi_H^{(\lambda-1,1)}}{dx} \right) \right] \cos^2 \phi = 0, \quad \text{(B3)}$$

$$\left[(\Theta - \Theta^{\star}) \frac{d\varphi_H^{(\lambda-1,1)}}{dx} + \left(\varphi_H^{(\lambda-1,1)} + \varphi_H^{(\lambda-1,2)} \right) \frac{d\Theta}{dx} + (\Theta + \Theta^{\star}) \frac{d\varphi_H^{(\lambda-1,2)}}{dx} \right] \cos^2 \phi$$

$$- \left[\varphi_H^{(\lambda-1,3)} \left(\frac{d\Theta^{\star}}{dx} - \frac{d\Theta}{dx} \right) + (\Theta^{\star} - \Theta) \frac{d\varphi_H^{(\lambda-1,3)}}{dx} \right] \frac{1}{2} \sin(2\phi)$$

$$+ \left[\frac{d\Theta^{\star}}{dx} \left(\varphi_H^{(\lambda-1,1)} + \varphi_H^{(\lambda-1,2)} \right) + \Theta \left(\frac{d\varphi_H^{(\lambda-1,2)}}{dx} - \frac{d\varphi_H^{(\lambda-1,1)}}{dx} \right) + \Theta^{\star} \left(\frac{d\varphi_H^{(\lambda-1,1)}}{dx} + \frac{d\varphi_H^{(\lambda-1,1)}}{dx} \right) \right] \sin^2 \phi$$

$$= 4\sqrt{2} v(x) \varphi_H^{(\lambda,2)}, \quad \text{(B4)}$$

$$\frac{1}{2} (\Theta - \Theta^{\star}) \sin(2\phi) \left[\frac{d\varphi_H^{(\lambda-1,1)}}{dx} - \frac{d\varphi_H^{(\lambda-1,2)}}{dx} \right] = \sqrt{2} v(x) \varphi_H^{(\lambda,3)}. \quad \text{(B5)}$$

Here, we also take into account the fact that $\langle \boldsymbol{v}_1 |$ itself is an eigenfunction of $\hat{\mathbb{O}}_T(x, p_y | \phi, \tau)$, and then

$$\langle \boldsymbol{v}_1 | \hat{\mathbb{O}}_T(x, p_y | \phi, \tau) | \boldsymbol{v}_{2,3} \rangle = \langle \boldsymbol{v}_{2,3} | \hat{\mathbb{O}}_T(x, p_y | \phi, \tau) | \boldsymbol{v}_1 \rangle = 0, \quad \text{(B6)}$$

which is simple because the transport operator $\hat{\mathbb{O}}_T(x, p_y | \phi, \tau)$ is Hermitian, i.e., $\hat{\mathbb{O}}_T(x, p_y | \phi, \tau) = \hat{\mathbb{O}}_T^{\dagger}(x, p_y | \phi, \tau)$.

In this paper, we will focus on the study of a dice lattice with $\phi = \pi/4$. From Eqs. (B3) to (B5), we obtain

$$-(\Theta + \Theta^{\star}) \left[\frac{d\varphi_H^{(\lambda-1,+)}}{dx} + \frac{d\varphi_H^{(\lambda-1,-)}}{dx} \right] - \left[\frac{d\Theta^{\star}}{dx} + \frac{d\Theta}{dx} \right] \varphi_H^{(\lambda-1,+)} - (\Theta - \Theta^{\star}) \frac{d\varphi_H^{(\lambda-1,3)}}{dx} + \left[\frac{d\Theta^{\star}}{dx} - \frac{d\Theta}{dx} \right] \varphi_H^{(\lambda-1,3)} = 0, \quad \text{(B7)}$$

$$(\Theta + \Theta^{\star}) \left[\frac{d\varphi_H^{(\lambda-1,+)}}{dx} - \frac{d\varphi_H^{(\lambda-1,-)}}{dx} \right] + \left[\frac{d\Theta^{\star}}{dx} + \frac{d\Theta}{dx} \right] \varphi_H^{(\lambda-1,+)}$$

$$+ (\Theta - \Theta^{\star}) \frac{d\varphi_H^{(\lambda-1,3)}}{dx} - \left[\frac{d\Theta^{\star}}{dx} - \frac{d\Theta}{dx} \right] \varphi_H^{(\lambda-1,3)} = 4\sqrt{2} v(x) \varphi_H^{(\lambda,2)}, \quad \text{(B8)}$$

$$(\Theta - \Theta^{\star}) \frac{d\varphi_H^{(\lambda-1,-)}}{dx} = \sqrt{2} v(x) \varphi_H^{(\lambda,3)}. \quad \text{(B9)}$$

[1] M. Vogl, O. Pankratov, and S. Shallcross, Phys. Rev. B **96**, 035442 (2017).

[2] N. Vandecasteele, A. Barreiro, M. Lazzeri, A. Bachtold, and F. Mauri, Phys. Rev. B **82**, 045416 (2010).

[3] Y. Zhang, Y. Barlas, and K. Yang, Phys. Rev. B **85**, 165423 (2012).

[4] N. Weekes, A. Iurov, L. Zhemchuzhna, G. Gumbs, and D. Huang, Phys. Rev. B **103**, 165429 (2021).

[5] V. Zalipaev, C. M. Linton, M. D. Croitoru, and A. Vagov, Phys. Rev. B **91**, 085405 (2015).

[6] V. Zalipaev, *Graphene: Synthesis, Characterization, Properties and Applications* (InTech, Rijeka, Croatia, 2011), p. 81.

[7] H. Berk, W. M. Nevins, and K. Roberts, J. Math. Phys. **23**, 988 (1982).

[8] E. Sonin, Phys. Rev. B **79**, 195438 (2009).

[9] F. Anwar, A. Iurov, D. Huang, G. Gumbs, and A. Sharma, Phys. Rev. B **101**, 115424 (2020).

[10] X. Ye, S.-S. Ke, X.-W. Du, Y. Guo, and H.-F. Lü, J. Low Temp. Phys. pp. 1–12 (2020).

[11] H.-Y. Xu and Y.-C. Lai, Phys. Rev. B **99**, 235403 (2019).

[12] S. A. H. Gangaraj, C. Valagiannopoulos, and F. Monticone, Phys. Rev. Res. **2**, 023180 (2020).

[13] P. Muratore-Ginanneschi, Phys. Rep. **383**, 299 (2003).

[14] A. Strohmaier and S. Zelditch, Advances in Mathematics **376**, 107434 (2021).

[15] E. B. Bogomolny and J. P. Keating, Phys. Rev. Lett. **77**, 1472 (1996).

[16] A. Kormanyos, P. Rakyta, L. Oroszlany, and J. Cserti, Phys. Rev. B **78**, 045430 (2008).

[17] R. G. Littlejohn and W. G. Flynn, Phys. Rev. Lett. **66**, 2839 (1991).

[18] R. G. Littlejohn and W. G. Flynn, Phys. Rev. A **44**, 5239 (1991).

[19] B. M. Karnakov and V. P. Krainov, *WKB Approximation in Atomic Physics* (Springer Science & Business Media, New York, 2012).

[20] V. P. Maslov, *The Complex WKB Method for Nonlinear Equations I: Linear Theory*, Vol. 16 (Springer Science & Business Media, New York, 1994).

[21] R. G. Littlejohn and J. M. Robbins, Phys. Rev. A **36**, 2953 (1987).

[22] G. Xiao-Yan and S. Jian-Qiang, Commun. Theor. Phys. **50**, 864 (2008).

[23] P. Delplace and G. Montambaux, Phys. Rev. B **82**, 205412 (2010).

[24] D. K. Kalluri, V. R. Goteti, and A. M. Sessler, IEEE Trans. Plasma Sci. **21**, 70 (1993).

[25] M. V. Berry and K. E. Mount, Rep. Prog. Phys. **35**, 315 (1972).

[26] D. Bercioux, D. F. Urban, H. Grabert, and W. Häusler, Phys. Rev. A **80**, 063603 (2009).

[27] B. Dóra, J. Kailasvuori, and R. Moessner, Phys. Rev. B **84**, 195422 (2011).

[28] J. Vidal, R. Mosseri, and B. Douçot, Phys. Rev. Lett. **81**, 5888 (1998).

[29] J. Vidal, P. Butaud, B. Douçot, and R. Mosseri, Phys. Rev. B **64**, 155306 (2001).

[30] E. Illes, Ph.D. thesis, University of Guelph, 2017.

[31] A. Iurov, G. Gumbs, and D. Huang, Phys. Rev. B **99**, 205135 (2019).

[32] B. Dey and T. K. Ghosh, Phys. Rev. B **98**, 075422 (2018).

[33] B. Dey and T. K. Ghosh, Phys. Rev. B **99**, 205429 (2019).

[34] N. Goldman and J. Dalibard, Phys. Rev. X **4**, 031027 (2014).

[35] A. Iurov, G. Gumbs, O. Roslyak, and D. Huang, J. Phys.: Condens. Matter **25**, 135502 (2013).

[36] K. Kristinsson, O. Kibis, S. Morina, and I. Shelykh, Sci. Rep. **6**, 20082 (2016).

[37] O. Kibis, Phys. Rev. B **81**, 165433 (2010).

[38] A. Iurov, L. Zhemchuzhna, G. Gumbs, and D. Huang, J. Appl. Phys. **122**, 124301 (2017).

[39] J. Sandoval-Santana, V. Ibarra-Sierra, A. Kunold, and G. G. Naumis, J. Appl. Phys. **127**, 234301 (2020).

[40] O. V. Kibis, K. Dini, I. V. Iorsh, and I. A. Shelykh, Phys. Rev. B **95**, 125401 (2017).

[41] O. Kibis, Phys. Rev. A **105**, 043106 (2022).

[42] S. M. Cunha, D. R. da Costa, J. M. Pereira, Jr., R. N. Costa Filho, B. Van Duppen, and F. M. Peeters, Phys. Rev. B **105**, 165402 (2022).

[43] J. D. Malcolm and E. J. Nicol, Phys. Rev. B **93**, 165433 (2016).

[44] A. Iurov, G. Gumbs, and D. Huang, J. Phys.: Condens. Matter **32**, 415303 (2020).

[45] Y. Abranyos, O. L. Berman, and G. Gumbs, Phys. Rev. B **102**, 155408 (2020).

[46] S. K. Firoz Islam and P. Dutta, Phys. Rev. B **96**, 045418 (2017).

[47] D. Huang, A. Iurov, H.-Y. Xu, Y.-C. Lai, and G. Gumbs, Phys. Rev. B **99**, 245412 (2019).

[48] S. M. Cunha, D. R. da Costa, J. M. Pereira, Jr., R. N. Costa Filho, B. Van Duppen, and F. M. Peeters, Phys. Rev. B **104**, 115409 (2021).

[49] A. Iurov, L. Zhemchuzhna, G. Gumbs, D. Huang, P. Fekete, F. Anwar, D. Dahal, and N. Weekes, Sci. Rep. **11**, 20577 (2021).

[50] D. F. Urban, D. Bercioux, M. Wimmer, and W. Häusler, Phys. Rev. B **84**, 115136 (2011).

[51] E. Illes and E. J. Nicol, Phys. Rev. B **95**, 235432 (2017).

[52] J. Wang, J. F. Liu, and C. S. Ting, Phys. Rev. B **101**, 205420 (2020).

[53] T. Louvet, P. Delplace, A. A. Fedorenko, and D. Carpentier, Phys. Rev. B **92**, 155116 (2015).

[54] C.-D. Han and Y.-C. Lai, Phys. Rev. B **105**, 155405 (2022).

[55] J. P. Carbotte, K. R. Bryenton, and E. J. Nicol, Phys. Rev. B **99**, 115406 (2019).

[56] A. Iurov, L. Zhemchuzhna, D. Dahal, G. Gumbs, and D. Huang, Phys. Rev. B **101**, 035129 (2020).

[57] Á. D. Kovács, G. Dávid, B. Dóra, and J. Cserti, Phys. Rev. B **95**, 035414 (2017).

[58] E. Illes, J. P. Carbotte, and E. J. Nicol, Phys. Rev. B **92**, 245410 (2015).

[59] E. Illes and E. J. Nicol, Phys. Rev. B **94**, 125435 (2016).

[60] A. Raoux, M. Morigi, J.-N. Fuchs, F. Piéchon, and G. Montambaux, Phys. Rev. Lett. **112**, 026402 (2014).

[61] F. Piéchon, J. Fuchs, A. Raoux, and G. Montambaux, in *Journal of Physics: Conference Series* (IOP, Bristol, England, 2015), Vol. 603, p. 012001.

[62] T. Biswas and T. K. Ghosh, J. Phys.: Condens. Matter **28**, 495302 (2016).

[63] T. Biswas and T. K. Ghosh, J. Phys.: Condens. Matter **30**, 075301 (2018).

[64] A. Balassis, D. Dahal, G. Gumbs, A. Iurov, D. Huang, and O. Roslyak, J. Phys.: Condens. Matter **32**, 485301 (2020).

[65] A. H. Castro Neto, F. Guinea, N. M. R. Peres, K. S. Novoselov, and A. K. Geim, Rev. Mod. Phys. **81**, 109 (2009).

[66] C.-Y. Tan, C.-X. Yan, Y.-H. Zhao, H. Guo, and H.-R. Chang, Phys. Rev. B **103**, 125425 (2021).

[67] S. Verma, A. Mawrie, and T. K. Ghosh, Phys. Rev. B **96**, 155418 (2017).

[68] A. E. Champo and G. G. Naumis, Phys. Rev. B **99**, 035415 (2019).

[69] S. K. Firoz Islam and A. Zyuzin, Phys. Rev. B **100**, 165302 (2019).

[70] S. K. Firoz Islam and A. Saha, Phys. Rev. B **98**, 235424 (2018).

[71] W.-X. Qiu, S. Li, J.-H. Gao, Y. Zhou, and F.-C. Zhang, Phys. Rev. B **94**, 241409 (2016).

[72] F. Wang and Y. Ran, Phys. Rev. B **84**, 241103(R) (2011).

[73] M. Orlita, D. Basko, M. Zholudev, F. Teppe, W. Knap, V. Gavrilenko, N. Mikhailov, S. Dvoretskii, P. Neugebauer, C. Faugeras *et al.*, Nat. Phys. **10**, 233 (2014).

[74] S. Ahmadkhani and M. V. Hosseini, J. Phys.: Condens. Matter **32**, 315504 (2020).

[75] G.-B. Jo, J. Guzman, C. K. Thomas, P. Hosur, A. Vishwanath, and D. M. Stamper-Kurn, Phys. Rev. Lett. **108**, 045305 (2012).

[76] J. Ruostekoski, Phys. Rev. Lett. **103**, 080406 (2009).

[77] L. Santos, M. A. Baranov, J. I. Cirac, H.-U. Everts, H. Fehrmann, and M. Lewenstein, Phys. Rev. Lett. **93**, 030601 (2004).

[78] X. Huang, Y. Lai, Z. H. Hang, H. Zheng, and C. Chan, Nat. Mater. **10**, 582 (2011).

[79] S. Mukherjee, A. Spracklen, D. Choudhury, N. Goldman, P. Öhberg, E. Andersson, and R. R. Thomson, Phys. Rev. Lett. **114**, 245504 (2015).

[80] Y. Li, S. Kita, P. Muñoz, O. Reshef, D. I. Vulis, M. Yin, M. Lončar, and E. Mazur, Nat. Photonics **9**, 738 (2015).

[81] R. A. Vicencio, C. Cantillano, L. Morales-Inostroza, B. Real, C. Mejía-Cortés, S. Weimann, A. Szameit, and M. I. Molina, Phys. Rev. Lett. **114**, 245503 (2015).

[82] T. Baba, Nat. Photonics **2**, 465 (2008).

[83] J. Romhányi, K. Penc, and R. Ganesh, Nat. Commun. **6**, 6805 (2015).

[84] N. A. Franchina Vergel, L. C. Post, D. Sciacca, M. Berthe, F. Vaurette, Y. Lambert, D. Yarekha, D. Troadec, C. Coinon, G. Fleury *et al.*, Nano Lett. **21**, 680 (2020).

[85] D. Leykam, A. Andreanov, and S. Flach, Adv. Phys.: X **3**, 1473052 (2018).

[86] A. Iurov, L. Zhemchuzhna, P. Fekete, G. Gumbs, and D. Huang, Phys. Rev. Res. **2**, 043245 (2020).

[87] Z. Li, T. Cao, M. Wu, and S. G. Louie, Nano Lett. **17**, 2280 (2017).

[88] E. V. Gorbar, V. P. Gusynin, and D. O. Oriekhov, Phys. Rev. B **99**, 155124 (2019).

[89] E. V. Gorbar, V. P. Gusynin, and D. O. Oriekhov, Phys. Rev. B **103**, 155155 (2021).